# New Substituted Polyacetylenes with Phenyleneethynylene Side Groups [−($C_6H_4$−C≡C)$_n$−$Si^iPr_3$; $n$ = 1, 2]: Synthesis, Characterization, Spectroscopic, and Photoelectric Properties

**Jiří Vohlídal,*,† Jan Sedláček, and Nikolay Patev**

*Department of Physical and Macromolecular Chemistry, Laboratory of Specialty Polymers,‡ Faculty of Science, Charles University, Albertov 2030, CZ-128 40 Prague 2, Czech Republic*

**Olivier Lavastre, Pierre H. Dixneuf, and Sandrine Cabioch**

*Laboratoire de Chimie de Coordination et Catalyse, UMR 6509 CNRS−Université de Rennes, Campus de Beaulieu, F-35042 Rennes, France*

**Hynek Balcar**

*J. Heyrovský Institute of Physical Chemistry, Academy of Sciences of the Czech Republic, Dolejškova 3, CZ-182 23 Prague 8, Czech Republic*

**Jiří Pfleger**

*Institute of Macromolecular Chemistry, Academy of Sciences of the Czech Republic, Heyrovského nám. 2, CZ-162 06 Prague 6, Czech Republic*

**Vratislav Blechta**

*Institute of Chemical Process Fundamentals, Academy of Sciences of the Czech Republic, CZ-165 02 Prague 6 - Suchdol, Czech Republic*

*Received April 15, 1999*

ABSTRACT: The selective, terminal triple bond polymerization of HC≡C−$C_6H_4$−C≡C−$Si^iPr_3$ (**1**) and HC≡C−$C_6H_4$−C≡C−$C_6H_4$−C≡C−$Si^iPr_3$ (**2**) yields soluble, high-MW polyacetylenes **P1** and **P2** with phenyleneethynylene-type pendant chains. The [Rh(cod)($OCH_3$)]$_2$- and $MoCl_5$-based catalysts show 100% polymerization selectivity to terminal triple bonds and give high-cis (NMR: Rh, 94% cis; Mo, 70% cis) polymers having a medium extent of $\pi$-conjugation. $WOCl_4$-based catalysts reacting in benzene marginally also insert internal triple bonds and give low-cis polymers (<10% cis) having a high extent of conjugation. Addition of 1,4-dioxane to the $WOCl_4$-based catalyst considerably reduces or even eliminates the internal triple bond insertion and increases the polymer molecular weight, cis-unit content (≈35% cis) and extent of $\pi$-conjugation. The $\pi$−$\pi$* band of **P1** pendant groups is closely correlated with the polymer microstructure: the cis-unit content in **P1** can be reliably ascertained from the $A_{292}/A_{268}$ UV-absorbance ratio. Raman bands of the main-chain $\nu$(C═C) mode exhibit both frequency and intensity dispersion with extent of conjugation. On the other hand, only intensity dispersion is conclusively observed for the $\nu$-(Ph−$C_{chain}$) band at 1341 $cm^{-1}$ that, upon correction to the dispersion effect, is in a good correlation with the cis-unit content obtained from NMR spectra. Xerographic and transient photoconductivity measurements have shown that the photogeneration in these polymers proceeds through the side group excited states, and the charge carrier's (holes) transport is controlled by hopping between the main chain conjugated sequences.

## Introduction

Substituted acetylene polymers are of interest due to their potential applicability as functional materials for electronic devices.[1−9] These polymers exhibit photoconductivity originating from their ability to capture, transport and mediate mutual conversions of the charges and energy and third-order nonlinear optical effects resulting from their increased higher-order optical susceptibility. In addition, conjugated oligomers of this type are applicable as molecular wires transporting charge and/or energy (signals) through membranes of supramolecular systems.[10] Actually, carotenoid pigments, like carotenes and zeaxanthines, which act as molecular wires in living systems, belong to the family of conjugated oligomers of substituted acetylenes. Therefore, the research on synthesis and properties of substituted acetylene polymers meets material demands of future electronics based on molecular and supramolecular devices.

Functional properties of substituted acetylene polymers depend on energy levels in macromolecules and the extent of their main chain conjugation, which can be tuned by the polymer molecular architecture (structure of substituents, regularity and configurational structure of macromolecules, distortion of main chains induced by steric effects of substituents, etc.). Rational tuning of photoelectrical properties of substituted polyacetylenes requires a good knowledge of processes underlying these functional properties, that is, the mechanism of charge carrier photogeneration and transport in these materials and relations between these properties and the polymer structure. In this respect,

† E-mail: vohlidal@prfdec.natur.cuni.cz.

‡ Supported by the Ministry of Education of the Czech Republic, Project 97103.

10.1021/ma9905829 CCC: $18.00 
Published on Web 09/18/1999

**Scheme 1. Modes of Polymerization of Monosubstituted Acetylenes**

**COORDINATION POLYMERIZATION** - formation of monosubstituted polyacetylenes

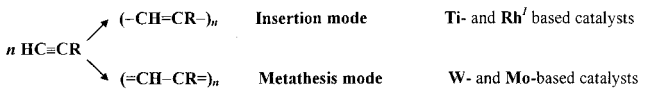


**POLYCONDENSATION** - formation of poly(aryleneethynylene)s


there is still a lack of detailed information, in particular, on the role of side groups and main chain conjugated sequences in these partial processes.[1−3,7−9]

Monoarylacetylenes can be transformed into conjugated substituted polyacetylenes by a chain polymerization induced with insertion or metathesis catalysts,[4,7,11] or into conjugated polymers containing main chain triple bonds, poly(aryleneethynylene)s,[12−15] via coupling reactions catalyzed with Pd or Pd/Cu complexes (see Scheme 1).

A combination of these two processes, i.e., the selective coordination polymerization of an oligomeric aryleneethynylene possessing terminal ethynyl (monomer prepared by coupling reactions, see, e.g., refs 16 and 17) taking place at terminal ethynyls only, should yield a substituted polyacetylene carrying conjugated, rodlike aryleneethynylene side chains of various lengths. Properties of such polymers might be tuned by both the side chain length and arylene ring substitution. Para substitution of the last side-chain ring should be preferred to avoid too high a diversity of steric effects. Such polymers can be useful in solving some problems related to the primary photogeneration and transport of charge carriers in substituted polyacetylenes. For example, if the charge carriers are mainly transported via conjugated side chains, they should have higher mobility in the polymer with longer side chains due to both a higher concentration and a greater extent of conjugation of these transport sites. However, if charge carriers are transported via main chains, they should be more mobile in the polymer with shorter side chains in which the average distance between hopping sites is lower. Further, the side chain extent of conjugation can affect the primary photogeneration process, etc.

The outlined synthetic approach has recently been used for a preparation of polyacetylenes carrying phenyleneethynylene pendant chains capped with ferrocenyl groups (Fc): $[-HC{=}C(-C_6H_4-C{\equiv}C-C_6H_4-C{\equiv}C-Fc)-]_n$[18] and $[-HC{=}C(-C_6H_4-C{\equiv}C-Fc)-]_n$.[19] However, both originally soluble polymers slowly become insoluble when stored in the solid state, which effect has been assigned to a cross-linking induced by the ferrocenyl groups.[19] Therefore, replacing the Fc groups with trialkylsilyl groups can be suggested to obtain more stable polymers suitable for the above physical investigation.

In the present paper, we report (i) the selective polymerization of (4-triisopropylsilylethynyl)phenylacetylene, $HC{\equiv}C-C_6H_4-C{\equiv}C-Si^iPr_3$ (**1**), and 4-[4-(triisopropylsilylethynyl)phenylethynyl]phenylacetylene, $HC{\equiv}C-C_6H_4-C{\equiv}C-C_6H_4-C{\equiv}C-Si^iPr_3$, (**2**), induced with various Rh-, Mo- and W-based catalysts, (ii) structure characterization of the respective polymers **P1** and **P2** on the basis of NMR, UV/vis, FT-Raman, and IR spectra, and (iii) a comparison of photoelectrical properties of **P1, P2**, and a reference sample of poly(phenylacetylene), PPA, prepared in the same way.

## Experimental Section

**Materials.** $WOCl_4$, tetraphenyltin ($Ph_4Sn$), phenylacetylene (all from Aldrich), benzene, and 1,4-dioxane (both Lachema, Czech Republic) were purified as described earlier.[20−22] $MoCl_5$, $RhCl_3{\cdot}3H_2O$, tetrabutyltin ($Bu_4Sn$), norbornadiene, cyclooctadiene, lithium phenylacetylide (1 M solution in THF) (all purchased by Aldrich), sodium carbonate, sodium, and methanol and other solvents (all purchased by Lachema, Czech Republic) were used as supplied. Tetrahydrofuran, (THF), (Riedel-DeHaen, purity 99.5%+) was distilled from $Cu_2Cl_2$ and $CaH_2$ and stored under argon atmosphere. Preparation of monomers **1** and **2** is described elsewhere.[16] Rhodium complexes, bis(triphenylphosphino)($\eta^4$-norbornadiene) rhodium(I) phenylacetylide, $[Rh(nbd)(PPh_3)_2(C{\equiv}CPh)]$, and bis($\mu$-methoxo)bis($\eta^4$-cycloocta-1,5-diene)dirhodium(I), $[Rh(cod)(OCH_3)]_2$, were prepared from $RhCl_3{\cdot}3H_2O$ according to procedures described in refs 23−25.

**Polymerizations.** Polymerizations induced with W- and Mo-based catalysts were carried out by using the standard vacuum break-seal technique and the following reaction conditions: [catalyst] = 3.3 mmol/L, [monomer] = 170 mmol/L, benzene as the main solvent, reaction time 24 h, and room temperature. Polymerizations induced with single-component $WOCl_4$ and $MoCl_5$ catalysts were simply started by mixing a benzene solution (2 mL) of **1** (141 mg, 0.5 mmol) or **2** (191 mg, 0.5 mmol) with the respective catalyst solution (1 mL, concentrated 10 mmol/L). If a cocatalyst ($Ph_4Sn$ or $Bu_4Sn$, see Table 1) was used, the catalyst solution (1 mL, concentrated 10 mmol/L) was first mixed with an equimolar amount, in the case of Mo-based catalyst, or twice that amount, in the case of the W-based catalyst, of the cocatalyst dissolved in benzene (0.5 mL), and after 15 min of ripening, the catalyst solution was mixed with the monomer (0.5 mmol in 1.5 mL of benzene). If dioxane (1.5 mL) cosolvent was used, it was added to the ripe $WOCl_4/2Ph_4Sn$ catalyst system (15 min in 1.5 mL of benzene), and after a further 15 min, the catalyst solution was mixed with the particular monomer (0.5 mmol) dissolved in ca. 0.2 mL of solvents distilled from the catalyst solution.[22] Polymerizations induced with Rh complexes were carried out under argon atmosphere by mixing THF solutions of the catalyst (1 mL, concentrated 10 mmol/L) and monomer (0.5 mmol in 2 mL THF). Polymerizations of **1** were quenched by pouring the reaction mixture (3 mL) into methanol (12 mL) because a majority of the oligomers was found to be soluble in the resulting solvent mixture. Precipitated polymer (**P1**) was filtered off and three times washed with methanol (25 mL). To remove oligomers from **P2,** polymerizations of **2** were quenched by pouring the reaction mixture (3 mL) into the methanol/benzene mixture (5:3 by volume, 12 mL) and the insoluble fraction was five times washed with the methanol/benzene mixture (2 mL, 1:1 by volume). Isolated polymers (**P*n***, where ***n*** = **1** or **2**) were dried in a vacuum to the constant weight and their yields determined by gravimetry. Supernatants from **P*n*** isolation were stripped of solvents and analyzed by SEC to determine the overall monomer conversion and the yield of oligomers.

**Polymer Characterization Methods. NMR spectra** were recorded on a Varian Unity 500 instrument operating at 499.843 MHz for $^1H$, 125.697 MHz for $^{13}C$, and 99.303 MHz for $^{29}Si$ using samples dissolved in $CDCl_3$ and hexamethyldisilane (1%, v/v) for referencing $^1H$ ($\delta = +0.04$ ppm) and $^{29}Si$ ($\delta = -19.79$ ppm) spectra. The $^{13}C$ spectra were referenced to the solvent ($\delta = +76.99$ ppm). Relaxation delay was set to 5 s. Signals of protonated and nonprotonated carbons were distinguished by the APT (attached proton test) method with the *J*-modulation period minimized by $^{13}C$ and $^1H$ refocusing pulses. The $^{29}Si$ spectra were acquisited by INEPT (insensitive nuclei enhanced by polarization transfer) with the polarization and refocusing delay experimentally optimized (by using the monomer) to 0.075 and 0.016 s, respectively.

**Table 1. Polymerization Data**[a]

| catalyst no. | catalyst formula | $x_M$, % | $Y_P$, % (color) | high-MW fraction, % pol. | $10^{-3}\langle M_{ap}\rangle_w$ | $10^{-3}\langle M_{ap}\rangle_n$ |
|---|---|---|---|---|---|---|
| | | | **P1** | | | |
| 1 | $WOCl_4$ | 96 | 75 (or.) | 2 | 120[b] | 65[b] |
| 2 | $WOCl_4/2Ph_4Sn$ | > 99 | 93 (or.) | 10 | 190[b] | 78[b] |
| 3 | $WOCl_4/2Ph_4Sn$/Diox | 72 | 67 (or.) | 0 | 220 | 110 |
| 4 | $WOCl_4/2Ph_4Sn$/Diox[c,d] | 86 | 84 (or.) | 0 | 350 | 140 |
| 5 | $MoCl_5$ | 60 | 39 (yel.) | 0 | 94 | 49 |
| 6 | $MoCl_5$[c] | 67 | 44 (yel.) | 0 | 101 | 49 |
| 7 | $MoCl_5/Bu_4Sn$ | 75 | 48 (yel.) | 0 | 113 | 59 |
| 8 | $MoCl_5/Ph_4Sn$ | 50 | 30 (yel.) | 0 | 88 | 49 |
| 9 | Rh(*nbd*)$(PPh_3)_2(C{\equiv}CPh)$[e] | 5 | oligomers | 0 | | |
| 10 | [Rh(*cod*)$(OCH_3)]_2$[e] | 99 | 89 (yel.) | 0 | 150 | 31 |
| | | | **P2** | | | |
| 11 | $WOCl_4/2Ph_4Sn$ | 93 | 80 (red) | 19 | 89[b] | 45[b] |
| 12 | $WOCl_4/2Ph_4Sn$/Diox | 65 | 48 (red) | 4 | 218[b] | 104[b] |
| 13 | $MoCl_5/Bu_4Sn$ | 31 | 14 (yel.) | 0 | 27 | 17 |
| 14 | Rh(*nbd*)$(PPh_3)_2(C{\equiv}CPh)$[e] | 25 | 15 (yel.) | 0 | 285 | 77 |
| 15 | [Rh(*cod*)$(OCH_3)]_2$[e] | 67 | 44 (yel.) | 0 | 66 | 43 |

[a] Conditions: [catalyst] = 3.3 mmol/L; [monomer] = 0.17 mol/L; polymerization time 24 h; room temperature. Solvents: W- and Mo-based catalysts in benzene; Diox in benzene/dioxane 1:1 by volume; Rh catalysts in THF. Symbols: $x_M$, the monomer conversion; $Y_P$, polymer yield; $\langle M_{ap}\rangle_w$ weight-average and $\langle M_{ap}\rangle_n$ number-average molecular weight. Color: yel., yellow; or., orange. [b] High-MW fraction not involved. [c] New monomer batch. [d] Conditions: [monomer] = 0.68 mol/L; polymerization time 48 h. [e] Polymerization time 1 h.

**IR spectra** were measured by the diffuse reflectance technique with nondiluted, powdered samples using FTIR Nicolet 210 and ATI Matson Genesis Series FTIR spectrometers (128 scans at resolution 4 $cm^{-1}$).

**FT Raman spectra** were recorded on Bruker IFS 55/S Equinox spectrometer fitted with a quartz beam splitter and equipped with FRA 106/S FT-Raman module with a liquid nitrogen-cooled germanium detector. Samples were excited in a 180° arrangement with the defocused 1064 nm line of an air-cooled Nd:YAG near-IR laser using the laser power at the sample set as less than 30 mW. Spectra were collected using 256 scans and a resolution of 4 $cm^{-1}$.

**UV/vis** optical absorption spectra were recorded on a Hewlett-Packard 8452 diode-array spectrometer using quartz cuvettes (0.2 cm) and freshly distilled spectroscopic grade THF as solvent.

**Size exclusion chromatography,** SEC, analyses were made on a TSP (Thermo Separation Products, Florida, USA) chromatograph equipped with a UV detector operating at 254 nm. A series of two PL-gel columns (Mixed B and Mixed C, Polymer Laboratories Bristol, U.K.) and THF (flow rate 0.7 mL $min^{-1}$) were used. Molecular weight averages relative to the polystyrene standards are reported.

**Photoelectrical Measurements. The quantum efficiency of free charge carrier photogeneration,** $\eta$, was measured by the xerographic discharge method[26] on polymer thin films cast on stainless steel substrates. The films were prepared by the spin casting method under argon atmosphere using toluene solutions, and their thickness (0.5−3.5 $\mu$m) was controlled by the spinning rate and solution concentration. Cast layers were dried overnight under the argon atmosphere and then in a vacuum (pressure 10 Pa) at 320 K for 6 h to obtain homogeneous crushless films. In the xerographic measurements, the light exposure was derived from the UV−CAMAG lamp with band filters 254 and 366 nm; the irradiation intensity was $2 \times 10^{17}$ photon $m^{-2}$ $s^{-1}$ and $1 \times 10^{18}$ photon $m^{-2}$ $s^{-1}$, respectively. The surface potential was measured with a rotary electrodynamic condenser electrometer[27] with a time resolution of 25 ms. In each measuring cycle, the surface of the polymer film was charged in the dark by a corona charging method and, after several seconds, illuminated by a steady light source. The surface potential decay was monitored both in the dark and under illumination and the quantum efficiency $\eta$ was obtained in a standard way using the relation $\eta = [(\epsilon_0\epsilon_r)/(\boldsymbol{e}\Phi L)](dU/dt)_{t=t_o}$, where $\epsilon_0\epsilon_r$ is the permittivity of the polymer, $\boldsymbol{e}$ the unit charge, $L$ the film thickness, $\Phi$ the absorbed photon flux and $(dU/dt)_{t=t_o}$ the surface potential decay rate at the onset of the illumination. The obtained $\eta$ values were corrected for the dark surface potential decay. The measurements were accomplished under the emission-limited conditions, which was verified by independence of the $\eta$ values on the sample thickness. To minimize any influence of the trapped space charge, the sample was always illuminated by white light and allowed to discharge down to the zero surface potential value and allowed to relax in the dark for 5 min before a subsequent measuring cycle was started.

**Relative permittivity,** $\epsilon_r$, of polymers was obtained from capacitance measurements on sandwich type samples using a semiautomatic Tesla BM 525 bridge and frequency of 1 kHz. The samples were prepared by spin casting of a polymer film on ITO glass, and after drying, the film was covered by metal aluminum layer (electrode) using the vacuum deposition method. To avoid errors caused by the parasitic capacitance of electrode−polymer interfacial layer the capacitance, $C$, was measured at various film thickness, $L$, and electrode area, $A$. The permittivity was calculated from the slope of the plot of $1/C$ vs parameter $L/(\epsilon_0 A)$.

**Transient photoconductivity measurements** were carried out on the sandwich type samples. Sandwiched polymer was photoexcited through the transparent ITO electrode by a 3 ns pulse ($\lambda_{ex}$ = 333 nm) derived from a Nd:YAG/dye laser (Continuum). The induced photocurrent was measured in the serial electrical circuit consisting of the sample, power supply Keithley K230 and digitizing storage scope Hewlett-Packard 54510 B.

## Results and Discussion

In the following text, the catalyst system used in a particular polymer synthesis is denoted by the following extension: Rh for [Rh(cod)$(OCH_3)]_2$ in THF; Mo for $MoCl_5$-based catalysts in benzene; W for $WOCl_4$-based catalysts in benzene; WD for $WOCl_4/2Ph_4Sn$ catalyst in dioxane/benzene (1:1 by volume) mixture. For example, **P*n***/Mo denotes **P*n*** (***n*** = **1** or **2**) samples prepared with the $MoCl_5$-based catalysts, **P*n***/WD denotes **P*n*** samples prepared with the $WOCl_4/2Ph_4Sn$ catalyst in dioxane−benzene mixed solvent, etc.

**Polymerization of 1 and 2.** Experimental data concerning the polymerizations are summarized in Table 1. All polymerizations are homogeneous and the formed polymers are also quite soluble in THF and $CHCl_3$. Some polymerizations are accompanied by a formation of higher amounts of oligomers (the difference between $x_M$ and $Y_P$, see Table 1).

The overall monomer conversion, $x_M$, as well as the polymer yield, $Y_P$, and molecular weight is higher for

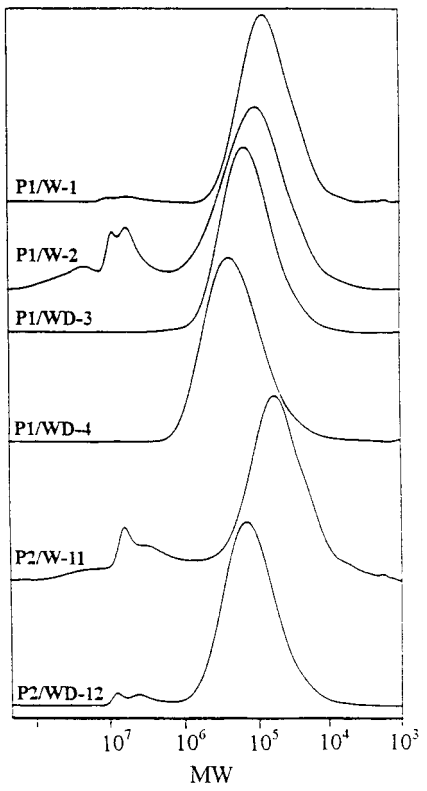


**Figure 1.** SEC traces of polymers prepared with $WOCl_4$-based catalysts: numbers are the sample numbers in Table 1.

polymerizations induced with $WOCl_4$-based catalysts compared to those induced with $MoCl_5$-based catalysts, the difference being more pronounced for **2** compared to **1**. Organotin cocatalysts have shown small effect on the activity of both types of catalysts. Similar observation has been reported for polymerizations of *p*-iodophenylacetylene.[28] Two examined Rh-based complexes show enormous difference in the polymerization activity. The most frequently used catalyst of this type, Rh(nbd)$(PPh_3)_2$(C≡CPh), is almost inactive in the polymerization of **1** but moderately active in polymerization of **2**. On the contrary, the $[Rh(cod)(OCH_3)]_2$ catalyst shows high polymerization activity with respect to **1** and only somewhat lower activity with respect to **2** (see Table 1).

Polymers prepared with $WOCl_4$-based catalysts mostly contain a soluble, high-MW fraction of the retention time at the upper exclusion limit (10 millions) of used SEC columns (see Figure 1 and Table 1—entries 1, 2, 11, and 12). The high-MW fraction can originate either from a marginal insertion of internal triple bonds (−C≡C− → >C=C<) or from the insertion of terminal ethynyls formed in a previous incidental desilylation of pendant-chain end groups (−Ph−C≡C−$Si^iPr_3$ → −Ph−C≡CH). The insertion of internal triple bonds seems to be the more justified mechanism for two reasons: (i) the content of high-MW fraction increases from **P1** to **P2,** i.e., as the number of internal triple bonds in monomer units increases, and (ii) a high-MW fraction also occurs in polymers of 4-(phenylethynyl)-phenylacetylene prepared with $WOCl_4$-based catalysts.[29] Accordingly, the absence of a high-MW fraction in **P*n***/Rh and **P*n***/Mo proves that growing species derived from $MoCl_5$- and Rh-based catalysts do not insert internal triple bonds, i.e., that these catalysts are more selective than the $WOCl_4$-based ones.

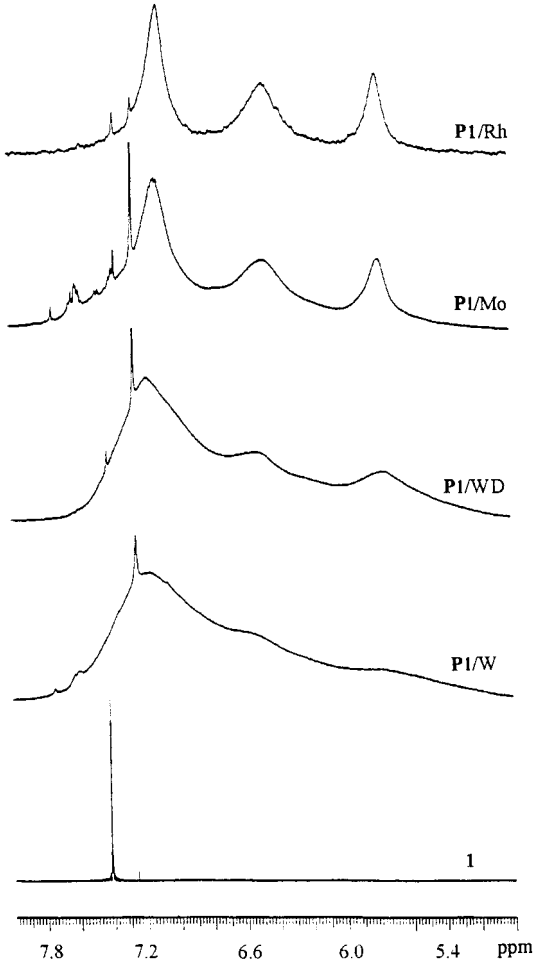


**Figure 2.** $^1H$ NMR spectra of monomer **1** and **P1** polymers (signal at 7.25 ppm is due to solvent, $CDCl_3$).

The addition of 1,4-dioxane cosolvent to $WOCl_4$-based catalyst system (i) eliminates the high-MW fraction formation in polymerization of **1**, (ii) substantially reduces formation of this fraction in the polymerization of **2**, and (iii) significantly increases the MW averages of formed **P*n*** (Table 1, entries 1−4, 11, and 12). The increase in polymer MW caused by addition of dioxane to tungsten-based polymerization catalysts has been reported for the reaction systems phenylacetylene−$WCl_6/Ph_4Sn$,[30] phenylacetylene−$WOCl_4/Ph_4Sn$,[20−22,31] and iodophenylacetylenes−$WOCl_4/Ph_4Sn$.[28,32] This effect was explained by a complexation of dioxane molecules with oxotungsten growing species, which results in hindering the species from termination.[28,32] 1,4-Dioxane is namely known to form well-defined coordination species with $WOCl_4$.[33] It suggests that binding of dioxane molecules to oxotungsten growing species reduces these species' ability to insert an internal triple bond, which consistently explains the here-observed suppression of the high-MW fraction formation upon addition of dioxane to $WOCl_4$-based catalyst systems.

**$^1H$ and $^{13}C$ NMR Spectra of P1 and P2.** NMR spectra of **P1** samples are shown in Figures 2 and 3 and the signals' assignment performed by using the APT method and NMR spectra of monomers[16] and various forms of poly(phenylacetylene), PPA,[34−42] is summarized in Table 2 for both **P1** and **P2** samples (for atom numbering, see Scheme 2). The disappearance of signals characteristic of terminal triple bonds (3.12 and 3.17

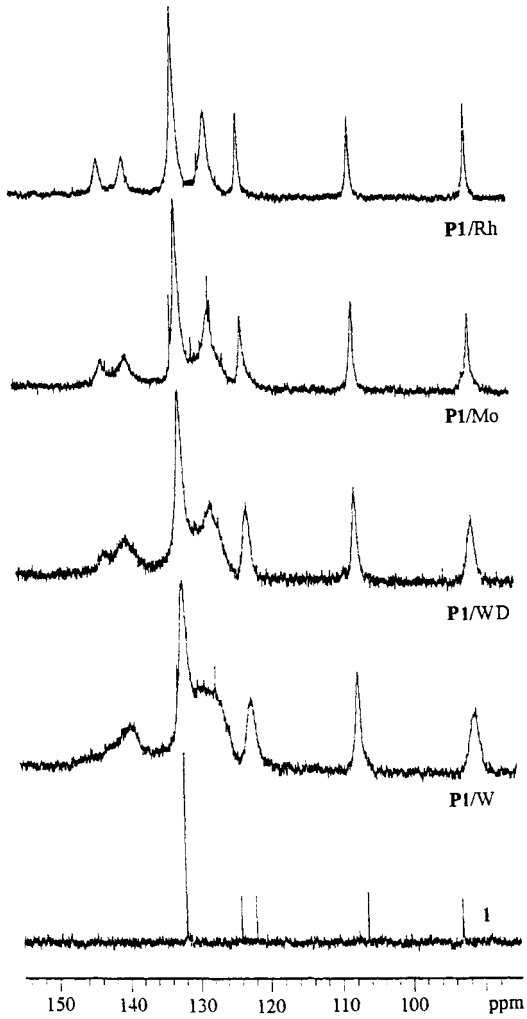


**Figure 3.** $^{13}$C NMR spectra of monomer **1** and **P1** polymers.

ppm, H1; 78.9 and 79.1 ppm, C1; 83.3 ppm, C2) and preservation of signals of internal triple bonds (at 107 ppm, C7; and at 90−93 ppm, C8, C7′, and C8′) demonstrate the high terminal-triple-bond selectivity of polymerizations. The shift of the C3 quaternary carbon signal from ca. 124 ppm in monomers to ca. 139 ppm in polymers and occurrence of new signals in the region typical of double bonds in PPAs (ca. 142 ppm for C2 and ca. 132 to 129.5 ppm for C1) demonstrate a presence of polyacetylene-type main chains in **P*n***. The absence of a $^1$H signal at 3.5 ppm proves that the polymers are virtually free of cyclohexadiene units.

According to the resolution of $^1$H and $^{13}$C NMR spectra as well as the half-width of the $^{29}$Si NMR signal of pendant groups, the microstructure uniformity of **P*n*** samples decreases in the following sequence: **P*n***/Rh > **P*n***/Mo > **P*n***/WD > **P*n***/W. Good resolved NMR spectra of **P*n***/Rh show main features characteristic of NMR spectra of PPAs prepared with $Rh^I$-based catalysts,[32,34,35,41,42] such that **P*n***/Rh samples can be assigned to the highly regular, head-to-tail (HT) cis−transoid polymers. Nevertheless, one feature of $^{13}$C NMR spectra needs an explanation. Apparently, the signal of the main-chain tertiary carbon C1′, which is found at 131.7 ppm in the PPA/Rh $^{13}$C NMR spectra, is missing in the spectra of **P*n***/Rh. However, approximately the same chemical shifts exhibit signals of the ring meta carbons C5—131.94 ppm for **1**, 131.78 ppm for **P1**/Rh, 132.04 ppm for **2**, 131.94 ppm for **P2**/Rh—which suggests that the C1′ carbon signal is merged with the signal of the ring meta carbons C5. Actually, when going from **P*n***/Rh to **P*n***/W, a new signal at ca. 129 ppm occurs in the $^{13}$C NMR spectra and increases in intensity on account of the signal intensity at 132 ppm, gradually filling the gap between signals at 132 and 127 ppm. These changes are consistent with the hypothesis that the signal of the C1′ carbon in HT-cis units occurs at 131.7 ppm and that the signal at 129 ppm belongs to C1′ carbons in trans units and/or irregular (HH−TT) sequences. This conclusion is further supported by the broadening of the C2′ signal at 142 ppm and its gradual merging with the C3 carbon signal at 139 ppm along the above sequence.

$^1$H NMR spectra of **P1**/Rh and **P1**/Mo consist of three peaks (main-chain H in cis units at 5.8 ppm, two *o*-H in cis units at 6.4 ppm, and two *m*-H at 7.1 ppm) with the line shape very close to the Lorentzian line. We utilized this fact for an assessment of peak areas by fitting the spectra with three Lorentzian lines using the line position, line width, and particular structure concentration as variable parameters. According to obtained areas (see Table 3), the **P1**/Rh sample contains ca. 94% cis units and the **P1**/Mo sample ca. 70% cis units. The content of cis units in **P1**/WD and **P1**/W samples could be ascertained only tentatively to ca. 35% and less than 10%, respectively.

**UV/vis Spectra.** Electronic spectra of **1** and **2** (Figures 4 and 5) are dominated by sharp doublets due to $\pi-\pi^*$ transitions in a unsaturated skeleton. Characteristics: $\lambda_{max}$ (molar absorption coefficient, $a$, in $10^3$ dm$^3$ mol$^{-1}$cm$^{-1}$): **1**, 286 nm (41.8), 272 nm (41.5), 214−218 nm (16.4); **2**, 338 nm (88.9), 316 nm (89.0), 220 nm (29.9) with a shoulder at 230 nm (ca 27). The doublet is also apparent but degenerated in UV spectra of **P1** samples (Figure 4) with the band maxima shifted to 292 nm ($a$ = 25.9 × $10^3$ dm$^3$ mol$^{-1}$ cm$^{-1}$ for **P1**/Rh) and 268 nm ($a$ = 26.1 × $10^3$ dm$^3$ mol$^{-1}$ cm$^{-1}$ for **P1**/W). As can be seen, the $A_{292}/A_{268}$ absorbance ratio is in a good correlation with the content of cis units ascertained from $^1$H NMR spectra (Figure 6). Thus, surprisingly, the main-chain configuration of a **P1** sample can be simply estimated from a measured value of the $A_{292}/A_{268}$ ratio of the main UV band. The analogous UV doublet structure is only poorly apparent in UV spectra of **P2** samples (Figure 5, $a$ ranges from 50 × $10^3$ to 60 × $10^3$ dm$^3$ mol$^{-1}$ cm$^{-1}$) such that it cannot be used for an estimate of the cis units content in **P2.**

According to the main-chain $\pi-\pi^*$ band intensity, the extent of $\pi$-conjugation in **P*n*** macromolecules descends in the sequence: **P*n***/WD ≥ **P*n***/W > **P*n***/Rh > **P*n***/Mo that differs from the cis-unit-content sequence established on the basis of the NMR spectra. Since all polymers are of the high-MW type (see Table 1), the extent of $\pi$-conjugation should be primarily controlled by the microstructure of their macromolecules. The cis units are known to act as weak conjugation defects in *trans*-polyacetylene chains,[1,43,44] so that one can expect conformity of the cis-unit-content and $\pi$-conjugation sample sequences. Therefore, the observed disparity of the sequences indicates a presence of other conjugation defects in **P*n*** macromolecules such as points of saturation and/or the HH−TT arrangement of monomeric units. The saturation defects are not clearly seen in the NMR spectra; however, a corresponding signal might be overlapped by signals of isopropyl groups. A presence of HH−TT sequences comes mainly into consideration

**Table 2. NMR Data for Monomers and Polymers**

| | **1** | **P1**/Rh | **P1**/Mo | **P1**/WD | **P1**/W | **2** | **P2**/Rh | **P2**/WD |
|---|---|---|---|---|---|---|---|---|
| | | | | Terminal Ethynyls of Monomers and Main Chain Atoms | | | | |
| H1 | 3.12 | 5.76 vs | 5.78 s | 5.79 m | 5.8 vw | 3.17 | 5.87 vs | 5.9 vw |
| C1 | 78.9 | 131.8 | 131.8 (129.5) | 132−129.5 | 129.5 | 79.06 | 131.38 | 131−129 |
| C2 | 83.3 | 142.5 | 142.5 | 143−136 | 145−135 | 83.25 | 142.14 | 142 |
| | | | | Phenylene Rings | | | | |
| H4 | 7.41 | 6.44 vs | 6.48 s | 6.5 m | 6.5 vw | 7.45−7.46 | 6.68 vs | 6.7 vw |
| H5 | 7.41 | 7.07 | 7.12 | 7.17 | 7.19 | 7.45−7.46 | 7.16 vs | not seen |
| H4′, H5′ | | | | | | 7.45−7.46 | 7.37 | 7.35 |
| C3 | 124.0 | 139.3 | 139.4 | 139.5 | 139.6 | 123.66 | 138.74 | 139 |
| C4 | 131.9 | 127 | 127 | 127 | 127 | 132.12 | 127.41 | 127 |
| C5 | 131.9 | 131.8 | 131.8 | 131.8 | 131.9 | 132.04 | 131.38 | 131.4 |
| C6 | 121.9 | 122.2 | 122.2 | 122.2 | 122.2 | 122.11 | 122.06 | 122 |
| C3′, C6′ | | | | | | 122.80, 123.55 | 123.07, 123.27 | 123.2 |
| C4′, C5′ | | | | | | 131.42, 131.50 | 131.94 | 131.4 |
| | | | | Internal Triple Bonds | | | | |
| C7 | 106.4 | 107 | 107 | 107 | 107 | 106.61 | 106.73 | 106.8 |
| C8 | 93.0 | 90.8 | 90.8 | 90.8 | 90.8 | 93.06 | 92.57 | 92.5 |
| C7′, C8′ | | | | | | 90.64, 91.12 | 90.05, 91.12 | 90.2, 91.2 |
| | | | | Triisopropylsilyl Group | | | | |
| H9, H10 | 1.12 | 1.10 | 1.10 | 1.11 | 1.12 | 1.11 | 1.10 | 1.11 |
| C9 | 11.32 | 11.28 | 11.28 | 11.28 | 11.32 | 11.33 | 11.30 | 11.27 |
| C10 | 18.70 | 18.68 | 18.68 | 18.67 | 18.67 | 18.70 | 18.66 | 18.64 |
| Si | −1.59 (2 Hz) | −1.74 (2 Hz) | −2.0 (20 Hz) | | −2.0 (60 Hz) | −1.64 (2 Hz) | −1.77 (2 Hz) | −2.0 (50 Hz) |

**Scheme 2. Reactions under Study and Structure and Numbering of Monomers and Polymers**

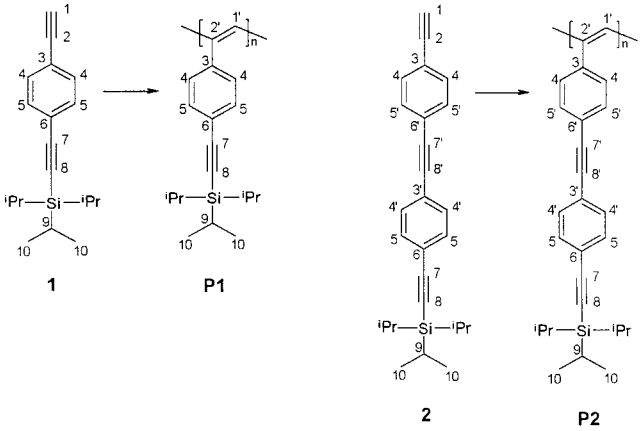


in the case of **P*n*** formed with a metathesis catalysts (viz., e.g., formation of head-to-head links in metatheses of olefins and alkynes[11]). Influence of the HH−TT sequences on the main chain conjugation is ambivalent. They should lower steric hindrances in the trans−transoid chains but considerably increase distortion of the cis−transoid chains as is obvious from the structures drawn in Figure 7. Accordingly, presence of the HH−TT cis−transoid units can be tentatively suggested as a reason for the lowered UV absorbance of **P*n***/Mo samples in the longer wavelength region. Unfortunately, an effective method for reliable determination of the head−tail isomerism of substituted polyacetylene macromolecules is still missing, although the first promising work in this field has appeared.[45]

**Off-Resonance Raman Spectra.** Raman bands of monomers can be assigned as follows. **1** (Figure 8): 2154 $cm^{-1}$, $\nu$(C≡CSi); 2111 $cm^{-1}$, $\nu$(C≡CH); 1604 $cm^{-1}$, $\nu$(C═C)$_{ring}$; 1222 $cm^{-1}$, $\delta_{ip}$(C−H); 1198 $cm^{-1}$, $\nu$(Ph−C$^{2}$≡); 1176 $cm^{-1}$, $\nu$(Ph−C$^{7}$≡); 885 and 837 $cm^{-1}$, $\delta_{oop}$(H−C═). **2**: 2215 $cm^{-1}$, $\nu$(PhC≡CPh); 2154 $cm^{-1}$, $\nu$(C≡CSi); 2110 $cm^{-1}$, $\nu$(C≡CH); 1597 $cm^{-1}$, $\nu$(C═C)$_{ring}$; 1223 $cm^{-1}$, $\delta_{ip}$(C−H); 1135 $cm^{-1}$, $\nu$(Ph−C$^{7'}$≡) and $\nu$(Ph−C$^{8'}$≡); 885 and 826 $cm^{-1}$, $\delta_{oop}$(H−C═). Valence bands of terminal ethynyls are absent while those of internal ethynyls are preserved in Raman spectra of **P1** and **P2**, which confirms the terminal-triple-bond selectivity of polymerizations.

Multiplets with maxima from ca. 1580 to 1500 $cm^{-1}$ in the Raman spectra of **P1** and **P2** belong to the $\nu$(C$^{1'}$═C$^{2'}$) main-chain skeletal vibrations (stretching of double bonds and contraction of single bonds). Both the overall intensity and width of this Raman band are in close correlation with the extent of $\pi$-conjugation of a particular **P*n*** sample (see Figures 4 and 8), which demonstrates the intensity and frequency dispersion of this band with the effective conjugation length.[1,43,44] The band at 1340 $cm^{-1}$ should be assigned to the $\nu$(Ph−C$^{2'}$)[46−49] stretching mode. This band shows the intensity dispersion but, entirely, no frequency dispersion with extent of conjugation same as the bands of $\delta_{ip}$(H−C$^{1'}$) and $\delta_{oop}$(H−C$^{1'}$) modes. To examine the influence of main chain microstructure on these bands, we corrected them with respect to the intensity dispersion effect, calculating the band intensity ratios $\nu$(Ph−C$^{2'}$)/$\nu$(C$^{1'}$ = C$^{2'}$), $\delta_{ip}$(H−C$^{1'}$)/$\nu$(C$^{1'}$ = C$^{2'}$), and $\delta_{oop}$(H−C$^{1'}$)/$\nu$(C$^{1'}$ = C$^{2'}$) using the following integration limits: 1590−1473 $cm^{-1}$ for $\nu$(C$^{1'}$ = C$^{2'}$), 1380−1315 $cm^{-1}$ for $\nu$(Ph−C$^{2'}$), 1290−1200 $cm^{-1}$ for $\delta_{ip}$(H−C$^{1'}$), and 930−820 $cm^{-1}$ for $\delta_{oop}$(H−C$^{1'}$). The $\delta_{ip}$(H−C$^{1'}$)/$\nu$(C$^{1'}$ = C$^{2'}$) and $\delta_{oop}$(H−C$^{1'}$)/$\nu$(C$^{1'}$ = C$^{2'}$) band-intensity ratios were found to be independent of the sample type being equal to 0.165 ± 0.015 and 0.11 ± 0.01, respectively. On the other hand, the $\nu$(Ph−C$^{2'}$)/$\nu$(C$^{1'}$═C$^{2'}$) band-intensity ratio shows a systematic course: 0.130 (**P1**/Rh) > 0.115 (**P1**/Mo) > 0.055 (**P1**/WD) > 0.035 (**P1**/W), which qualitatively obeys the cis-units content in **P1** samples ascertained from NMR spectra.

The $\nu$(Ph−C$^{2'}$) band at about 1340 $cm^{-1}$ is usually assigned to the cis units[46,47,49−51] because it is always intense in Raman spectra of PPAs and ring-substituted PPAs prepared with Rh(diene) complexes, which are believed to be the high-cis-HT polymers. However, this assignment is not unambiguous because, for example, the cis-to-trans isomerization of meta and para ring-iodinated PPAs[32] is accompanied by the intensity increase of the band at 1340 $cm^{-1}$. This points to the inconsistency of this band assignment to the cis struc-

**Table 3. Results of Fits of $^1$H NMR Spectra of P1 Samples with Lorentzian Lines**

| | **P1**/Rh | | | **P1**/Mo | | |
|---|---|---|---|---|---|---|
| | $H^5$ | $H^4$ | $H^1$ | $H^5$ | $H^4$ | $H^1$ |
| line position, ppm | 7.074 | 6.438 | 5.759 | 7.127 | 6.471 | 5.787 |
| line width, Hz | 80 | 157 | 65 | 149 | 207 | 84 |
| fraction of the $^1$H signal in unsaturated groups,[a] % | 41.6 (40) | 39.7 (40) | 18.7 (20) | 52 (40) | 34 (40) | 14 (20) |

[a] In parentheses is given the theoretical fraction of a particular signal for an ideal all-cis polymer.

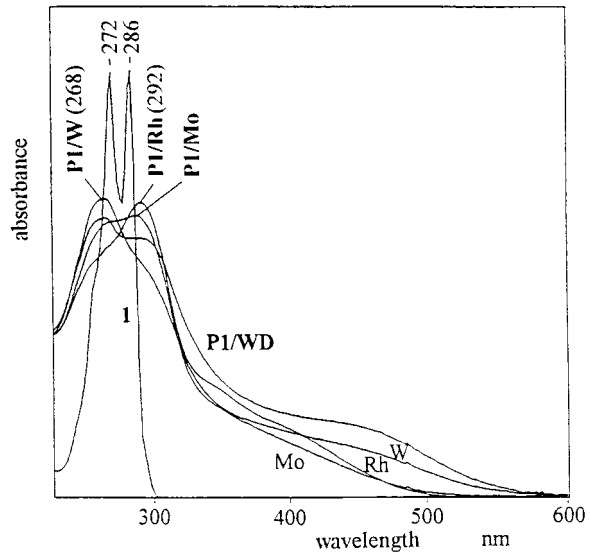


**Figure 4.** UV spectra of monomer **1** and **P1** polymers (for values of molar absorption coefficients, see text).

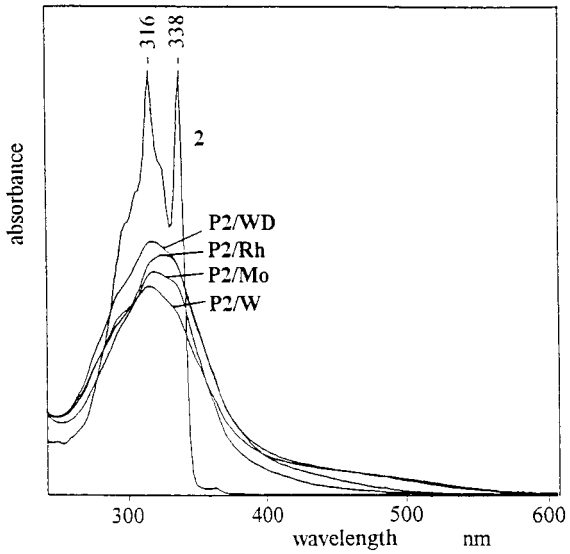


**Figure 5.** UV spectra of monomer **2** and **P2** polymers (for values of molar absorption coefficients see text).

ture. Therefore, this band can be alternatively assigned to the $\nu$(Ph−C$^{2'}$) mode in PPAs with main chains in the trapezoidal configuration,[32] i.e., to both the cis−transoid and trans−cisoid structures. Accordingly, the lowered intensity of this band points to an increased content of the zigzag (trans−transoid) configuration in **P1**/W and **P1**/WD macromolecules. However, this interpretation needs other supporting information.

**Infrared spectra** have confirmed the terminal triple bond selectivity of polymerizations. It is evidenced by the absence of the terminal triple bond bands at 3279 (vs) cm$^{-1}$ $\nu$(H−C≡) and 2108 (w) cm$^{-1}$ $\nu$(C≡CH) and the preservation of the internal triple bond $\nu$(C≡C) band

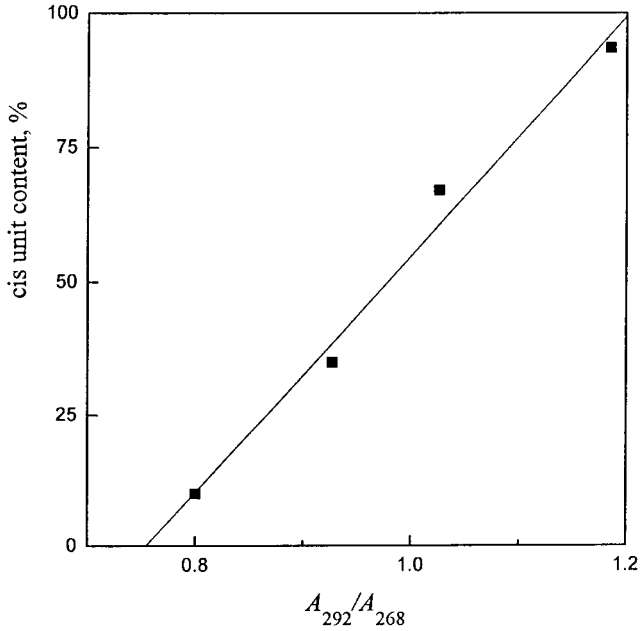


**Figure 6.** Correlation between the $A_{292}/A_{268}$ UV absorbance ratio and the cis unit content in **P1** samples ascertained by NMR spectra.

at 2152 cm$^{-1}$ in spectra of **P*n*** samples. On the other hand, only minor differences attributable to particular configurations are apparent in the IR spectra. The bands at 811(m), 782 (m), and 720 (w) cm$^{-1}$ can be tentatively assigned to the cis units because they are apparent in the **P1**/Rh spectrum and, with decreased intensity, also in the IR spectra of **P1**/Mo and **P1**/WD. On the other hand, the **P1**/W and **P1**/WD spectra show a weak band at 739 cm$^{-1}$ that is absent in IR spectra of **P1**/Mo and **P1**/Rh samples. Thus, this band can be assigned to the trans units. Similar but still less pronounced trends are apparent in IR spectra of **P2** samples. Other differences in IR spectra of **P*n*** samples are more complex; they cannot be clearly correlated with the cis-unit content and their conclusive interpretation is questionable.

**Photoelectrical properties** were investigated for samples of **P1**/WD and **P2**/WD that show the highest extent of main-chain $\pi$-conjugation and on the PPA/WD reference sample prepared in the same synthetic route.

Examples of the *surface potential dark decay and photoinduced discharge* curves for both positively and negatively charged surfaces of **P1**/WD and **P2**/WD films (thickness $L \sim 2.3$ $\mu$m) obtained at $F = 8 \times 10^7$ V m$^{-1}$ and $\lambda_{ex} = 254$ nm are shown in Figure 9. The curves are normalized to the value of surface potential $U_{s0}$ at the onset of illumination ($t = 0$). The curves in Figure 9 show that **P2**/WD exhibits both dark and photoinduced discharges that are faster compared to those for **P1**/WD. In addition, the curves indicate a presence of a nonnegligible residual surface potential, mainly in the case of negative charging. Faster discharging of the

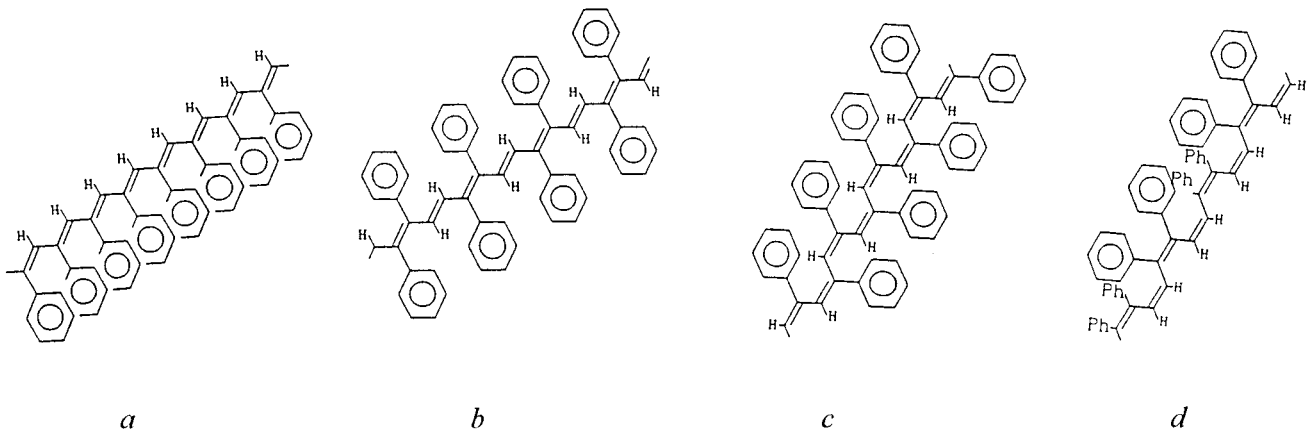


**Figure 7.** Steric hindrances in PPA chains: planar projections of PPA chains formed in the metathesis polymerization: (a) HT trans-transoid chain; (b) HH−TT trans−transoid chain; (c) HT cis−transoid chain; (d) HH-TT cis−transoid chain.

positively charged surfaces compared to negatively charged surfaces proves that holes are the majority charge carriers, being more mobile than photogenerated electrons in both **P1**/WD and **P2**/WD, the same as in the case of PPA/WD. Assuming that no injection of charge carriers occurs either from the polymer film surface or from the substrate, the xerographic discharge curves can be discussed in the following way. In the dark at zero external electric field, the polymer contains free and trapped charge carriers in thermal equilibrium concentrations that are controlled by the bulk thermal generation rate, free charge carrier lifetime, and trapping time. The free charge carriers are swept out from the sample under the influence of external electric field after corona charging, but the deeply trapped charges remain in the bulk as a space charge that slows down both the dark and photoinduced discharges. Thus, it can be concluded that (i) the thermal generation of charges is faster in **P2**/WD compared to **P1**/WD, and (ii) deep trapping of electrons is more probable than that of holes in both polymers.

The dependences of the *free charge carrier photogeneration efficiency*, $\eta$, on the electric field $F$ for positively charged films ($L = 0.8-3.5\ \mu$m) of **P1**/WD, **P2**/WD, and (reference) PPA/WD[52,53] samples as obtained at $\lambda_{ex}$ equal to 254 and 366 nm are shown in Figure 10. Intrinsic photogeneration of free charge carriers in conjugated polymers is an electric field and temperature-dependent multistep process that involves a creation of thermalized Coulombic-bound electron−hole pairs after photoexcitation and their subsequent dissociation into free charge carriers.[9,52,54] The overall free charge carrier photogeneration efficiency can be expressed as

$$\eta(F) = \eta_0 \int f(r,F)\, g(r)\, \mathrm{d}\tau \qquad (1)$$

where $\eta_0$ denotes the electric-field-independent primary quantum efficiency, i.e., the fraction of absorbed photons that results in a formation of thermallized charge pairs, $\mathrm{d}\tau$ is a volume element in spherical coordinates, and $f(r,F)$ is the electric-field-dependent probability of the charge pair dissociation given by the Onsager theory. The function $g(r)$ is the distribution of radii of charge pairs, which, in disordered systems such as amorphous polymers, can be described by the Gaussian distribution $g(r) \approx \exp(-r^2/\alpha^2)$, where $\alpha$ is the dispersion parameter that corresponds to the most probable distance from which the dissociation proceeds in the high electric field limit.

Fits of experimental data from Figure 10 by the formula in (1) provided values of parameters $\eta_0$ and $\alpha$ that are summarized in Table 4. As can be seen, the primary efficiency $\eta_0$ increases in the sequence **P1**/WD < **P2**/WD ≤ PPA/WD. The $\eta$ vs $F$ curves for excitation at 254 nm (energy above that of the side-group lowest absorption band) are parallel, which indicates that differences in $\eta$ are given by differences of $\eta_0$ values in this case. On the other hand, for 366 nm excitation (region of the substituent absorption edge), the curves have different slopes and differences in $\eta$ can be mainly ascribed to differences in the separation radii $\alpha$.

The above photogeneration efficiency sequence is inconsistent with the order of both the substituent bulkiness and extent of main chain conjugation. Further, the photogeneration efficiency $\eta_0$ in the studied samples increases as the excitation wavelength decreases, which is typical of substituted polyacetylenes.[6,7,9,52,53] The photogeneration threshold occurs at a considerably shorter wavelength than that one corresponding to the lowest lying electronic transition in these polymers. The absence of photoconductivity in the long wavelength region, where the main chain $\pi-\pi^*$ transition is active, can be explained by a very fast recombination of intrachain polaron−excitons. This implies that the primary photogeneration in substituted polyacetylenes takes place preferably on side groups and that the autoionization of an excited side group proceeds directly via an interchain charge transfer from the higher excited states without a preceding internal conversion to the LUMO state. As virtually all light is absorbed in the polymer surface layer, the primary photogeneration efficiency $\eta_0$ should be mainly controlled by the ability of excited side groups to undergo the interchain autoionization (viz. $\alpha$ that is above 1 nm). This ability should be independent of the main chain extent of conjugation as well as the side group bulkiness because the side group chemical constitution and their interactions with neighboring macromolecules must control it.

**Charge Carrier Mobility.** A typical transient photocurrent signal obtained with **P1**/WD sandwiched film ($L = 2.5\ \mu$m, applied voltage 200 V, room temperature) is shown in Figure 11. The signal shape proves the dispersive transport of charge carriers in a system of hopping sites randomly distributed on the energy and intersite-hopping distance scales. The hopping sites might be identified with the delocalized $\pi$-conjugated sequences in polymer main chains in which moving

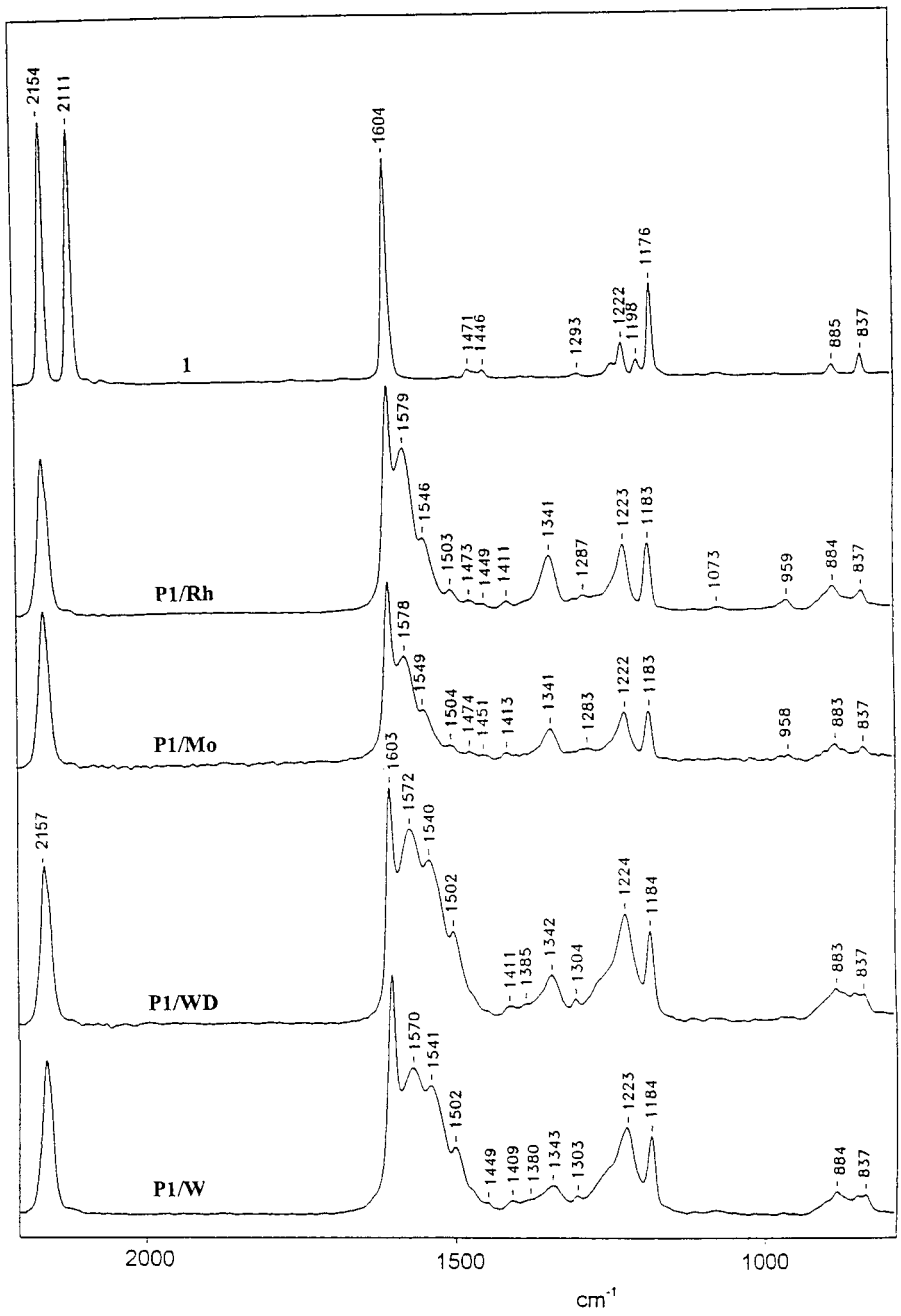


**Figure 8.** Off-resonance Raman spectra of monomer **1** and **P1** polymers.

holes can have the lowest possible energy. The dispersive transport of charge carrier is characterized by the mean charge carrier mobility, $\mu$, given as

$$\mu = L^2/(Ut_{tr}) \qquad (2)$$

where $U$ is the applied voltage and $t_{tr}$ the effective transit time of photogenerated charge carriers to the opposite electrode that is obtained as a time of the break on the double logarithmic plot of transient photocurrent vs time dependence (see Figure 11). Obtained values of $\mu$ are summarized in Table 4.

The value of $\mu$ decreases progressively in the order PPA > **P1** > **P2**, which can be clearly explained in terms of the influence of substituent bulkiness on the charge carrier mobility. Bulky substituents have two important structure effects: (i) they lower the average extent of main chain $\pi$-conjugation owing to the main chain distortion, and (ii) they increase the average distance between main chains. The former reduces the charge carrier intrachain mobility, whereas the latter decreases the probability of the charge carrier interchain hopping. Therefore, it seems that the conjugation within the phenyleneethynylene side chains, which is established on a higher energy level compared to the polyacetylenic main chains, has little effect on the interchain transport of charge carriers. Thus, it can be concluded that the charge carriers (holes) are transported by means of intersite hopping between the main chain conjugated sequences in the studied substituted polyacetylenes.

Summarizing the above, it can be suggested that a substituted polyacetylene exhibiting good photoconductivity should consist of main chains with the high extent of conjugation to which side groups with high primary photogeneration efficiency are attached.

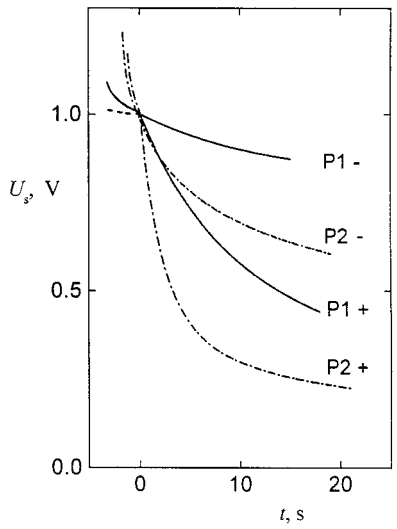


**Figure 9.** Surface potential dark decay and photoinduced discharge curves for positively and negatively charged surfaces of **P1**/WD and **P2**/WD films (thickness $L \sim 2.3$ $\mu$m) obtained at $F = 8 \times 10^7$ V m$^{-1}$ and $\lambda_{ex} = 254$ nm.

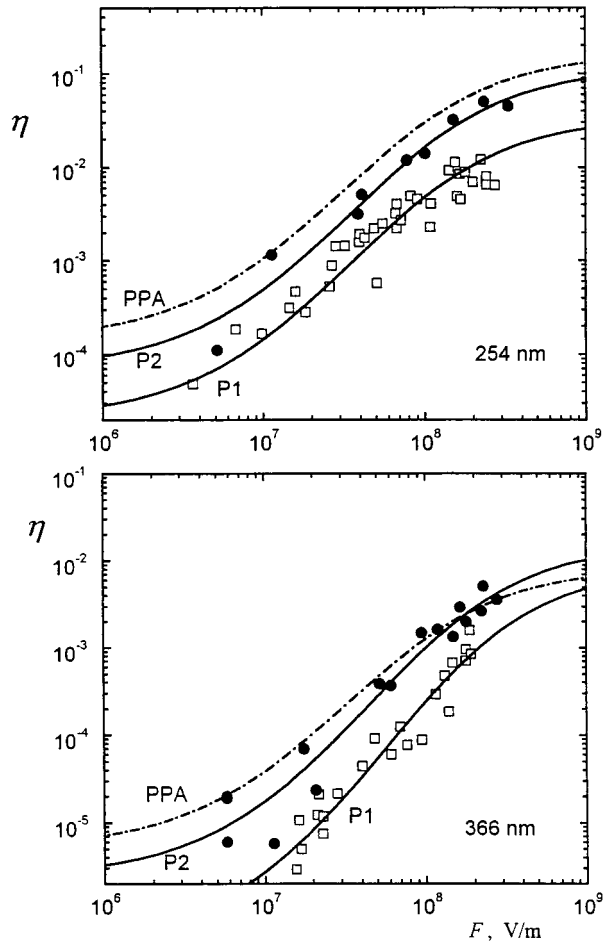


**Figure 10.** $\eta$ vs $F$ plots for positively charged films ($L = 0.8-3.5$ $\mu$m) of **P1**/WD, **P2**/WD and PPA/WD (reference) samples for $\lambda_{ex}$ equal to 254 and 366 nm.

**Acknowledgment.** The authors are very grateful to the Grant Agency of Charles University (189/97-B-CH), Grant Agency of Czech Academy of Sciences (A 1050901), French-Czech exchange program Barrande (1998/97085) and the Region Bretagne for financial support and to Dr. I. Němec (Department of Inorganic Chemistry, Charles University) and Dr. P. Matějka (Department of Analytical Chemistry, Prague Institute of Chemical Technology) for measuring the IR and Raman spectra.

**Table 4. Photoelectric and Dielectric Characteristics of P1/WD, P2/WD, and Reference PPA/WD Samples at Room Temperature**[a]

| | | | $\lambda_{ex} = 254$ nm | | $\lambda_{ex} = 366$ nm | |
|---|---|---|---|---|---|---|
| | $\epsilon_r$ | $\mu$, cm$^2$/(V s) | $\eta_0$, el./photon | $\alpha$, nm | $\eta_0$, el./photon | $\alpha$, nm |
| **P1**/WD | 3.3 | $1 \times 10^{-6}$ | 0.035 | 1.5 | 0.009 | 1.0 |
| **P2**/WD | 3.4 | $2 \times 10^{-7}$ | 0.12 | 1.5 | 0.016 | 1.2 |
| PPA/WD | 3.1 | $4 \times 10^{-5}$ | 0.15 | 1.7 | 0.009 | 1.6 |

[a] Key: $\epsilon_r$, relative permittivity; $\mu$, charge carrier (hole) mobility; $\eta_0$, photogeneration quantum efficiency; $\alpha$, dispersion parameter.

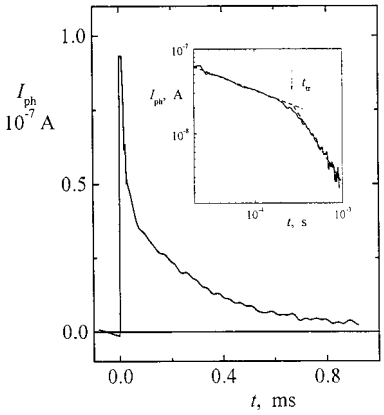


**Figure 11.** Transient photocurrent signal obtained with **P1**/WD sandwiched film, $L = 2.5$ $\mu$m, applied voltage 200 V, and room temperature. Inset: bilogarithmic plot for the determination of the effective transit time $t_{tr}$.

## References and Notes

(1) Chien, J. C. W. *Polyacetylene—Chemistry, Physics and Material Science*; Academic Press: New York, 1984.
(2) *Nonlinear Optical and Electroactive Polymers*; Prasad, P. N., Ulrich, D. R., Eds.; Plenum Press: New York, 1987.
(3) *Conjugated Polymers*; Brédas, J. L., Silbey, R., Eds.; Kluwer Academic Publishers: Dordrecht, The Netherlands, 1991.
(4) Shirakawa, H.; Masuda, T.; Takeda, K. In *The Chemistry of Triple-Bonded Functional Groups*; Patai, S., Ed.; Wiley: New York, 1994; Supplement C2, Chapter 17, pp 945−1016.
(5) Long, N. J. *Angew. Chem., Int. Ed. Engl.* **1995**, *34*, 21.
(6) *Photoactive Organic Materials*; Kajzar, F., Ed.; NATO ASI Series; Kluwer Academic Publishers: Dordrecht, The Netherlands, 1996.
(7) *Handbook of Organic Conductive Molecules and Polymers*; Nalwa, H. S., Ed.; Wiley: New York, 1996.
(8) Manners, L. I. *Angew. Chem., Int. Ed. Engl.* **1996**, *35*, 1602.
(9) Nešpůrek, S. In *Photoactive Organic Materials*; Kajzar, F., Ed.; NATO ASI Series; Kluwer Academic Publishers: Dordrecht, The Netherlands, 1996; pp 411−430.
(10) Benniston, A. C.; Goule, V. C.; Harriman, A.; Lehn, J.-M.; Marczinke, B. *J. Chem. Phys.* **1994**, *98*, 7798.
(11) Ivin, K. J.; Mol, J. C. *Olefin Metathesis and Metathesis Polymerization*; Academic Press: London, 1997.
(12) Heck, F. R. *Palladium Reagents in Organic Synthesis*; Academic Press: London, 1990.
(13) Giesa, R. *J. Macromol. Sci. Macromol. Chem. Phys.* **1996**, *C36*, 631.
(14) Lavastre, O.; Plass, J.; Bachmann, P.; Guesmi, S.; Moinet, C.; Dixneuf, P. H. *Organometallics* **1997**, *16*, 184.
(15) Yamamoto, T.; Morikita, T.; Maruyama, T.; Kubota, K.; Katada, M. *Macromolecules* **1997**, *30*, 5390.
(16) Lavastre, O.; Ollivier, L.; Dixneuf, P. H.; Sibandhit, S. *Tetrahedron* **1996**, *52*, 5495.
(17) Lavastre, O.; Cabioch, S.; Dixneuf, P. H.; Vohlídal, J. *Tetrahedron* **1997**, *53*, 7595.
(18) Buchmeiser, M. R. *Macromolecules* **1997**, *30*, 2274.

(19) Sedláček, J.; Vohlídal, J.; Patev, N.; Cabioch, S.; Lavastre, O.; Dixneuf, P. H.; Balcar, H.; Matějka, P. *Macromol. Chem. Phys.* **1999**, *200*, 972.
(20) Vohlídal, J.; Rédrová D.; Pacovská, M.; Sedláček, J. *Collect. Czech. Chem. Commun.* **1993,** *58*, 2651.
(21) Sedláček, J.; Vohlídal, J.; Grubišic-Gallot, Z. *Makromol. Chem. Rapid Commun.* **1993**, *14*, 51.
(22) Šedláček, J.; Pacovská, M.; Vohlídal, J.; Grubišic-Gallot, Z.; Žigon, M. *Macromol. Chem. Phys.* **1995**, *196*, 1705.
(23) Chatt, J.; Venanzi, L. M. *J. Chem. Soc.* **1957**, 4735.
(24) Kishimoto, I.; Eckerle, P.; Miyatake, T.; Ikariya, T.; Noyori, R. *J. Am. Chem. Soc.* **1994**, *119*, 12131.
(25) Connelly, N. G.; Loyns, A. C.; Fernandez, M. J.; Modrego, J.; Oro, L. A. *J. Chem. Soc., Dalton Trans.* **1989**, 683.
(26) Chen, I.; Mort, J.; Tabak, M. D. *IEEE Trans. Electron Devices* **1972**, *19*, 413.
(27) Nešpůrek, S.; Ulbert, K. *Čs. čas. fyz.* **1975**, *25A*, 144.
(28) Vohlídal, J.; Sedláček, J.; Pacovská, M.; Lavastre, O.; Dixneuf, P. H.; Balcar, H.; Pfleger, J. *Polymer* **1997**, *38*, 3359.
(29) (a) Vohlídal, J.; Sedláček, J.; Patev, N.; Balcar, H.; Cabioch, S.; Lavastre, O.; Dixneuf, P. H. *Proceedings of the International Symposium on Metathesis and Related Chemistry, ISOM 12*; St. Augustine, FL, July 13−18, 1997; p 97. (b) Cabioch, S. Transformations catalytiques de molécules insaturées en polymeres conjugués. Thesis, Université de Rennes 1, France, September 1998.
(30) Masuda, T.; Takahashi, T.; Yamamoto, K.; Higashimura, T. *J. Polym. Sci., Polym. Chem. Ed.* **1982**, *20*, 2603.
(31) Sedláček, J.; Vohlídal, J.; Kareš, J.; Pacovská, M.; Máca, B. *Collect. Czech. Chem. Commun.* **1994**, *59*, 2454.
(32) Vohlídal, J.; Sedláček, J.; Patev, N.; Pacovská, M.; Cabioch, S.; Lavastre, O.; Dixneuf, P. H.; Blechta, V.; Matějka, P.; Balcar, H. *Collect. Czech. Chem. Commun.* **1998**, *63*, 1815.
(33) Fowles, G. W. A.; Frost, J. L. *J. Chem. Soc. A, Inorg. Phys. Theor.* **1967**, 671.
(34) Furlani, A.; Napoletano, C.; Russo, M. V.; Feast, J. W. *Polym. Bull.* **1986**, *16*, 311.
(35) Tabata, M.; Yang, W.; Yokota, K. *J. Polym. Sci., Polym. Chem.* **1994**, *32*, 1113.
(36) Simionescu, C. I.; Percec, V.; Dimitrescu, S. *J. Polym. Sci., Polym. Chem. Ed.* **1977**, *15*, 2497.
(37) Percec, V. *Polym. Bull.* **1983**, *10*, 1.
(38) Percec, V.; Rinaldi, P. L. *Polym. Bull.* **1983**, *9*, 548.
(39) Sanford, T. J.; Allendoerfer, R. D.; Kang, E. T.; Ehrlich, P. *J. Polym. Sci., Polym. Phys. Ed.* **1980**, *18*, 2277.
(40) Sanford, T. J.; Allendoerfer, R. D.; Kang, E. T.; Ehrlich, P.; Schaefer, J. *J. Polym. Sci., Polym. Phys. Ed.* **1981**, *19*, 1151.
(41) Kishimoto, I.; Miyatake, T.; Ikariya, T.; Noyori, R. *Macromolecules* **1996**, *29*, 5054.
(42) Hirao, K.; Ishii, Y.; Terao, T.; Kishimoto, I.; Miyatake, T.; Ikariya, T.; Noyori, R. *Macromolecules* **1998**, *31*, 3405.
(43) Gussoni, M.; Castiglioni, C.; Zebri, G. In *Spectroscopy of Advanced Materials*; Clark, R. J. H., Hester, R. E., Eds.; Wiley: New York, 1991; Chapter 5, pp 251−353.
(44) Zebri, G.; Gussoni, M.; Castiglioni, C. In *Conjugated Polymers*; Brédas, J. L., Silbey, R., Eds.; Kluwer Academic Publishers: Dordrecht, The Netherlands, 1991; pp 435−507.
(45) Duc, S.; Petit, A. *J. Anal. Appl. Pyrolysis* **1997**, *40−41*, 55.
(46) Tabata, M.; Sone, T.; Sadahiro, Y.; Yokota, K. *Macromol. Chem. Phys.* **1998**, *199*, 1161.
(47) Tabata, M.; Tanaka, Y.; Sadahiro, Y.; Sone, T.; Yokota, K.; Miura, I. *Macromolecules* **1997**, *30*, 5200.
(48) Lefrant, S.; Lichtman, L. S.; Temkin, H.; Fitchen, D. B.; Miller, D. C.; Whitwell, G. E.; Burlitch, J. M. *Solid State Commun.* **1979**, *29*, 191.
(49) Tabata, M.; Nozaki, Y.; Yokota, K. *J. Photopolym. Sci. Technol.* **1993**, *6*, 1.
(50) Tabata, M.; Namioka, M.; Yokota, K.; Minakawa, H. *Polymer* **1998**, *37*, 1959.
(51) Tabata, M.; Kobayashi, S.; Sadahiro, Y.; Nazaki, Y.; Yokota, K.; Yang, W. *J. Macromol. Sci., Pure Appl. Chem.* **1997**, *A34*, 641.
(52) Pfleger, J.; Nešpůrek, S.; Vohlídal, J. *Mol. Cryst. Liq. Cryst.* **1989**, *166*, 143.
(53) Kminek, I.; Cimrova, V.; Nešpůrek, S.; Vohlídal, J. *Makromol. Chem.* **1989**, *190*, 1025.
(54) Onsager, L. *Phys. Rev.* **1938**, *54*, 554.

MA9905829